Crystallographic, magnetic and electronic structures of a new layered ferromagnetic compound $Cr_2Ge_2Te_6$

1995 J. Phys.: Condens. Matter 7 69

(http://iopscience.iop.org/0953-8984/7/1/008)

J. Phys.: Condens. Matter 7 (1995) 69–87. Printed in the UK

Crystallographic, magnetic and electronic structures of a new layered ferromagnetic compound $Cr_2Ge_2Te_6$

V Carteaux†§, D Brunet‡, G Ouvrard‡ and G André†

† Laboratoire Léon Brillouin, CEA–CNRS, Centre d'Etudes de Saclay, 91191 Gif sur Yvette Cédex, France

‡ Laboratoire de Chimie des Solides, IMN, UMR 110, CNRS, 2 rue de la Houssinière, 44072 Nantes Cédex 03, France

Received 31 May 1994

Abstract. $Cr_2Ge_2Te_6$ is a new layered material belonging to the lamellar ternary $M_2X_2Te_6$ chalcogenides family (where M is a 3^+ oxidation state metal and X_2 a silicon or a germanium pair). It was synthesized from a stoichiometric mixture of the elements and heated in a sealed evacuated quartz tube for 20 d at 700 °C. The crystal symmetry is rhombohedral, of space group $R\bar{3}$, with the following hexagonal cell parameters: $a = b = 0.682\,75(4)$ nm, $c = 2.056\,19(9)$ nm, $V = 0.830\,1(1)$ nm^3 and $Z = 3$. The crystal structure of $Cr_2Ge_2Te_6$ was solved using both x-ray single-crystal diffraction and neutron powder diffraction data. Growth defects were detected and investigated using high-resolution electron microscopy. The magnetic structure and properties of $Cr_2Ge_2Te_6$ have been determined by neutron powder diffraction and susceptibility and magnetization measurements. Below 61 K, $Cr_2Ge_2Te_6$ is ferromagnetic with spins aligned along the c axis of the cell ($\mu(Cr^{3+}) = 2.80(4)\mu_B$ at 5 K). The thermal evolution of the magnetic moments below T_C is given. At room temperature, $Cr_2Ge_2Te_6$ presents a $\rho = 0.02\ \Omega$ cm resistivity. Above T_C, the thermal evolution of the resistivity can be fitted as $\rho = \exp(A/kT)$, where $A = 0.2$ eV. Band-structure and crystal orbitals of $Cr_2Ge_2Te_6$ have been calculated using the extended Hückel method and indicate no gap but highly localized Cr 3d states, giving evidence of a hopping mechanism for $Cr_2Ge_2Te_6$ electrical conductivity.

1. Introduction

Low-dimensional transition-metal chalcogenides have been largely studied for their anisotropic physical properties. Among them, lamellar transition-metal chalcogenophosphates MPX_3 (M ≡ V, Mn, Fe, Co, Ni, Zn, Cd or Hg; X ≡ S or Se) present a great variety of compounds which allows one to investigate deeply the influence of the nature of the transition-metal atom on the magnetic properties [1]. Various substitutions have been considered in these compounds but to date no tellurophosphate has been obtained. A few years ago an isostructural tellurosilicate $Cr_2Si_2Te_6$ was prepared and characterized [2]. Its structure can be described from a hexagonal compact stacking of tellurium atoms in which chromium atoms and silicon pairs occupy octahedra in every other slab. The empty slab is identified as the so-called van der Waals gap. Chromium atoms and silicon pairs are ordered inside the slab and from one slab to the adjacent slabs in a way inducing rhombohedral symmetry, usually described in a hexagonal cell ($a = b = 0.675\,78(6)$ nm, $c = 2.066\,5(1)$ nm and $V = 0.817\,3(2)$ nm^3). The chromium tellurosilicate evidences interesting physical properties with a ferromagnetic ordering below 32 K [3] and a non-metallic behaviour [4].

§ Author to whom correspondence should be addressed.

0953-8984/95/010069+19$19.50

In order to determine the influence of the nature of the chalcogen and the post-transition element on the structural and physical characteristics of the chromium ternary chalcogenides, various substitutions have been envisaged. In this field, pseudo-one-dimensional $CrSbSe_3$ [5] and $CrSbS_3$ [6] and two-dimensional $Cr_2Sn_3Se_7$ [7] have been recently obtained. In this paper we report the synthesis of the parent chromium tellurogermanate $Cr_2Ge_2Te_6$. Its crystallographic and magnetic structures have been determined using x-ray, electron and neutron diffraction techniques. The magnetic properties of this new phase are described in relation to its structure and by comparison with the parent chromium tellurosilicate.

2. Experimental details

$Cr_2Ge_2Te_6$ was prepared by heating a stoichiometric mixture of the elements in a sealed evacuated quartz tube to 700 °C for 20 d, followed by cooling for 10 h. A fine dark-grey crystalline powder was obtained, in the bulk of which small hexagonal single-crystal platelets were found. The inner quartz tube container was found to be very clean. Energy-dispersive spectroscopy, performed on single crystals, yielded typically the chemical formula $Cr_{2.2}Ge_{1.9}Te_{5.9}$, in good agreement with the expected 2:2:6 stoichiometry. This corresponds also to stoichiometry of the bulk. No other phase was detected using energy-dispersive spectroscopy (performed with an EDAX-equipped JEOL-JSM35C scanning electron microscope), or x-ray and neutron diffraction. The single crystals found in the $Cr_2Ge_2Te_6$ powder present typically edges of a few tenths of a millimetre, which is too small for resistivity measurements. This led us to grow some larger crystals using high-temperature solution growth (because of the thermal dissociation of $Cr_2Ge_2Te_6$, melt growth techniques could not be easily applied). Single crystals up to a centimetre size were yielded by coalescence of powdery $Cr_2Ge_2Te_6$ in a tellurium flux at 700 °C within 100 h ($Cr_2Ge_2Te_6$, molar ratio 1:30), followed by very slow cooling (5 °C h^{-1}). The advantage of tellurium as the flux medium is that no intermediate or other solid phases are stable in the liquid.

Hexagonal symmetry and cell parameters were first established on single crystals by film methods (rotating-crystal and Weissenberg photographs), leading to $a = b = 0.683$ nm and $c = 2.061$ nm. The cell constants were refined from an x-ray powder diffraction diagram, using a least-squares program [8], to $a = b = 0.682\,75(4)$ nm, $c = 2.056\,19(9)$ nm and $V = 0.830\,1(1)$ nm^3. This powder diffraction diagram was obtained using a CPS 120 INEL diffractometer (Cu $K\alpha_1$ radiation) and with silicon as internal standard. Table 1 shows the observed and calculated d_{hkl} interplanar distances with their intensities. As preferential orientation is often observed for lamellar compounds, we also present the 'theoretical' intensities calculated with the Lazy Pulverix program [9]. Single-crystal x-ray diffraction data were collected on a four-circle CaD4 Enraf–Nonius diffractometer. The MoLEN Software package (1991 version) distributed by Enraf–Nonius [10] was used to solve the structure.

Between 4.2 and 300 K, the magnetic susceptibility was measured by the Faraday method. Magnetization measurements were performed on either a 'home-made' vibrating-sample magnetometer or a SQUID (Quantum Design), in the temperature range 4.2–300 K. Neutron diffraction patterns were collected on the G4.1 powder diffractometer of the high-flux reactor of the Laboratoire Léon Brillouin at Saclay, using a wavelength of 0.2425 nm. This diffractometer is equipped with a position-sensitive detector (PSD) recording simultaneously 80° in 2θ. The sample container was an aluminium can of 10 mm diameter, held in an aluminium liquid-helium cryostat. After the absence of diffraction peaks at very small angles in the magnetic phase was proved, the PSD was positioned to record diffraction

Table 1. Observed and calculated interplanar distances for $Cr_2Ge_2Te_6$.

d_{obs} (nm)	d_{calc} (nm)	hkl	$100I/I_0$	I (Lazy Pulverix)
6.85	6.85	003	10	10
3.426	3.426	006	46	37
3.055	3.056	113	100	100
2.923	2.926	021	5	4
2.418	2.418	116	20	10
1.970	1.970	300	30	31
1.898	1.898	119	31	16
1.713	1.713	0012	11	5
1.708	1.708	306	19	9
1.656	1.656	223	13	10
1.3673	1.3673	229	7	2
1.2931	1.2931	3012	9	3
1.2721	1.2720	1115	13	5
1.2680	1.2680	413	9	2
1.2075	1.2075	416	2	<1
1.1376	1.1379	330	4	2
1.12333	1.12349	419	5	1
1.08324	1.08325	1118	4	1
0.93944	0.93953	4115	1	<1

diagrams in the range $17° < 2\theta < 97°$. Patterns were collected at various temperatures between 5 K and the Curie temperature, in order to detect possible anomalies in the thermal behaviour of the magnetic moment. Finally, longer data acquisitions were performed above T_C (for 70, 85, 110, 200 and 270 K) to record information on the paramagnetic state. Resistivity measurements were performed on $Cr_2Ge_2Te_6$ platelets, using both the van der Pauw [11, 12] method (for measurements of room-temperature resistivity) and the Montgomery [13] method (to study the thermal evolution of the resistivity).

3. Crystal structure determination

Considering that $Cr_2Ge_2Te_6$ presents the same stoichiometry, a very close chemical formula and cell parameters highly comparable with those of $Cr_2Si_2Te_6$, we first thought that the two silicon and germanium derivatives would certainly be isostructural. In fact, close examination of a rotating crystal exposed for a long time and Weissenberg photographs of $Cr_2Ge_2Te_6$ single crystals indicate that, besides the bright Bragg spots corresponding to the rhombohedral existence law $-h+k+l = 3n$, far less intense spots were also observed, which disobey this law and thus disagree with the expected rhombohedral symmetry. As proof that this was not due to a poor-quality twinned crystal, we chose several single crystals within the bulk of the $Cr_2Ge_2Te_6$ powder, but the same phenomenon was observed for each of them. A single-crystal structure determination was made using a four-circle diffractometer, leading to a lower trigonal symmetry (space group, P312) for $Cr_2Ge_2Te_6$ crystals. Anyway, several characteristics of this single-crystal refinement were found to be not fully satisfactory, and a neutron powder structure determination, using ground and 50 μm screened $Cr_2Ge_2Te_6$ powder, was also performed, in order to verify the crystallographic structure. However, the analysis of powder neutron diffraction diagrams using the Rietveld method led to a rhombohedral $R\bar{3}$ symmetry. Both structure determinations are described below, and their results discussed in comparison with each other.

3.1. X-ray single-crystal structure determination

A suitably sized single crystal was easily found for the x-ray diffraction data collection. Because of the large linear absorption coefficient ($\mu = 314.4\ cm^{-1}$), an absorption correction was made, using the empirical absorption correction method program of Walker and Stuart [14]. Table 2 shows the experimental conditions for data collection and structure calculation.

Table 2. Data collection and structure calculations for $Cr_2Ge_2Te_6$ single crystals.

Physical and crystallographic data	
Chemical formula	$Cr_2Ge_2Te_6$
Molecular mass	1014.81 g mol^{-1}
Colour	Medium grey
Crystal symmetry	Trigonal
Space group	P312
Cell parameters at 293 K (refined using x-ray INEL diffractometer powder data)	
a	0.682 75(4) nm
b	0.687 75(4) nm
c	2.056 19(9) nm
V	0.830 1(1) nm^3
Z	3
Calculated density d_{calc}	6.091 g cm^{-3}
Linear absorption coefficient $\mu(\lambda_{Mo\ K\alpha})$	313.4 cm^{-1}
Data collection	
Temperature	293 K
Radiation	Mo Kα, $\lambda = 0.071\,069$ nm
Monochromator	Graphite 002
of scan mode	1.5–30°, ω–2θ
Values for the scan speed	
σ_{pre}	0.7
σ	0.01
v_{pre}	7° min^{-1}
t_{max}	60 s
Standard reflections	(0 6 12), (4 $\bar{2}$ 7), (0 0 12)
Refinement conditions	
Number of reflections recorded in $\frac{1}{4}$ space	1928
Number of independent reflections $I > 3\sigma(I)$	640
Number of refined parameters	19
Reliability factors	
R	0.053
R_w	0.046
Extinction coefficient E_c	$7.0(4) \times 10^{-8}$
Residual charge density	$3.9(7) \times 10^3$ e^- nm^{-3}

Considering that $Cr_2Ge_2Te_6$ is trigonal, and that centrosymmetry tests indicate a non-centrosymmetric structure, a P3 space group was used as the starting group for the refinement. Then, the cationic distribution between chromium atoms and germanium pairs was determined using successive Fourier-difference calculations and least-squares refinement cycles and led to the P312 space group. Refinements with three tellurium atoms Te(1), Te(2) and Te(3), positioned on 6(1) sites, first led to a reliability factor $R = 0.23$. Then, introducing germanium pairs on 2g sites (Ge(1)) and 2h sites (Ge(2) and Ge(3)), and

chromium atoms on 2g sites (Cr(1)), 2i sites (Cr(2)), 1d sites (Cr(3)) and 1f sites (Cr(4)) led to the final values $R = 0.053$ and $R_w = 0.046$, with isotropic temperature factors and secondary extinction coefficients taken into account. Because non-stoichiometry is always possible in this type of layered chalcogenide phases, some refinement cycles were conducted with various occupancies of the anion sites and also the cation sites, resulting in no significant differences.

The temperature factors of the atoms were not anisotropically refined, because of divergence of thermal factors when anisotropy is introduced. On the other hand, the values of the isotropic thermal factors of the same type of atoms exhibit strong dispersion but compensate each other; so we constrained them to be identical for atoms of the same type. Furthermore, the final Fourier-difference map yielded quite a high residual electronic density of 3.9×10^3 e^- nm^3. Such problems could be due to a wrong space group choice, but all other possibilities were checked; considering the specific cationic distribution obtained for $Cr_2Ge_2Te_6$ single crystals, and according to the Hamilton [15] test, P312 is the only convenient group. However, residual high coefficients in the correlation matrix indicate that the crystal structure is not perfectly described using the P312 trigonal space group. Furthermore, the refinement problems for the thermal factors and the high residual electronic density could certainly be related to structural defects. This point will be examined in detail in section 3.3.

As for its silicon derivative, $Cr_2Ge_2Te_6$ is a layered material constructed from an ABAB hexagonal close packing of tellurium atoms. One of each two octahedral site planes is empty, and the other is filled orderly with germanium pairs and Cr^{3+} ions in a 1:2 ratio (figure 1(*a*)). For the single-crystal trigonal structure, the slabs are stacked in such a way that the $(\frac{2}{3}\frac{1}{3}z)$ cationic position is never occupied by a germanium pair (figure 1(*b*)), owing to their high Z, tellurium atoms are usually well positioned during crystal structure determinations. Furthermore, the fact that the same ABAB hexagonal compact anion stacking is found for $Cr_2Ge_2Te_6$ as for its parent silicon derivative (and for all other known $MXTe_3$ compounds [16, 17]) left few doubts about the tellurium atom positions. On the other hand, according to the high final residual electronic density, some uncertainty remains about the cationic distribution within the slab, and from one slab to another. Assuming that these structure determination problems were due to structural growth defects (as stacking faults and twinning are often observed for the parent MPX_3 (X ≡ S or Se) compounds [18]) led us to determine the powdery $Cr_2Ge_2Te_6$ structure, using neutron diffraction powder patterns. As the $Cr_2Ge_2Te_6$ single-crystal structure corresponds to a 'faulted' structure, the position coordinates of atoms are not reliable and are not given.

3.2. Neutron powder diffraction

The neutron powder diffraction diagram recorded at room temperature was analysed using the Rietveld–Hewat [19, 20] method and led to the rhombohedral $R\bar{3}$ symmetry for the $Cr_2Ge_2Te_6$ structure. The data collection and refinement parameters are listed in table 3. A Gaussian shape was found to be convenient to describe the Bragg peaks. Successive least-squares cycles using the Fullprof program [21] led to the following reliability factors: $R_{exp} = 0.0505$, Bragg R-factor=0.0621 and R_F factor=0.0537 (conventional Rietveld factors $R_p = 0.177$, $R_{wp} = 0.179$ and $R_e = 0.0505$), and to the atomic positions listed in table 4. As for single crystals, the structure is based on an ABAB stacking of tellurium hexagonal planes. Between these anionic planes, one plane is left empty (constituting the so-called van der Waals gap), and the other is filled orderly, one third by germanium pairs, and two thirds by chromium atoms. Cationic distributions within the slab are found to be the same for powder and single crystals of $Cr_2Ge_2Te_6$. The only difference appearing

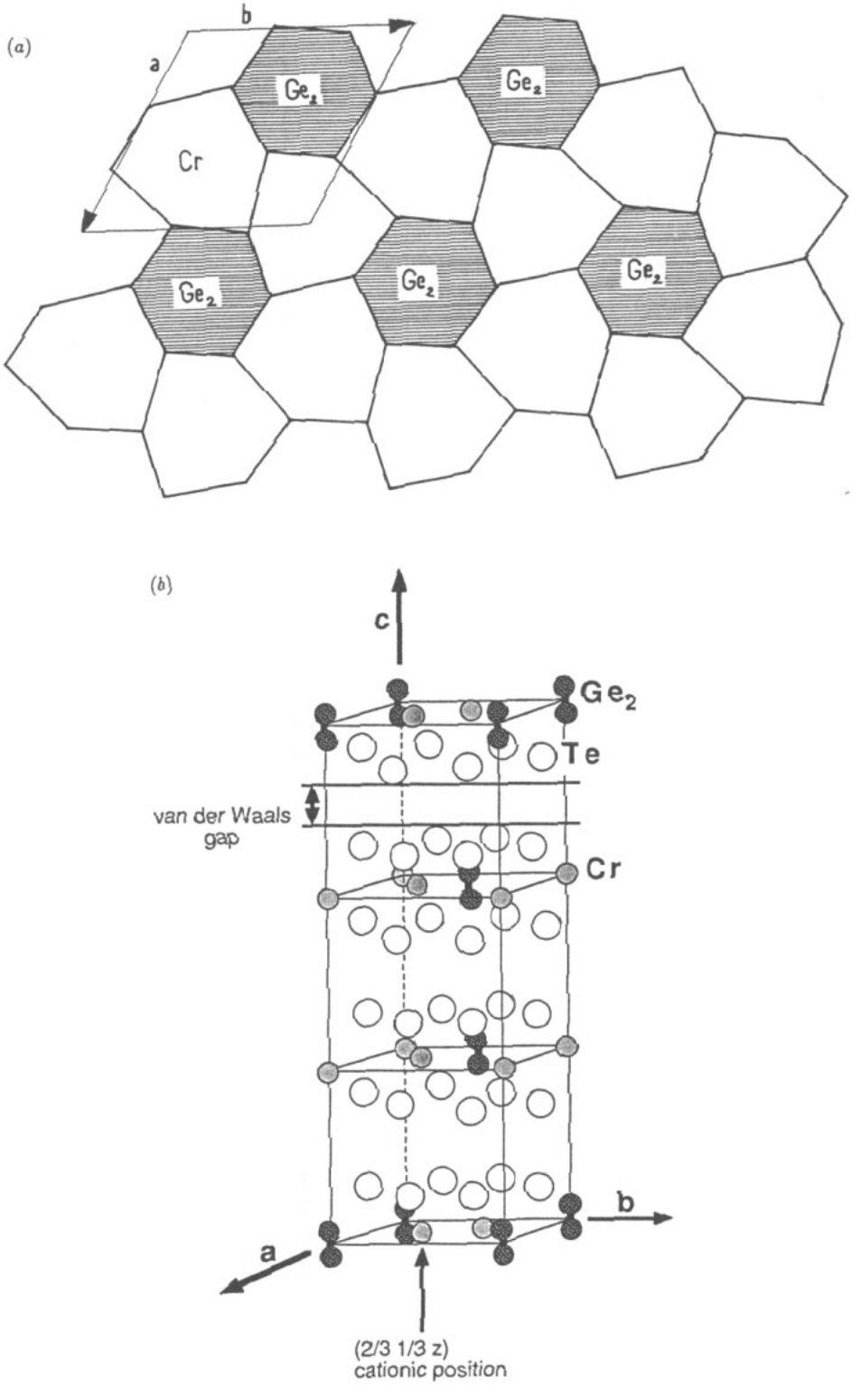
(a)
b
a
Ge2
Ge2
Cr
Ge2
Ge2
Ge2
(b)
c
Ge2
Te
van der Waals gap
Cr
b
a
(2/3 1/3 z)
cationic position

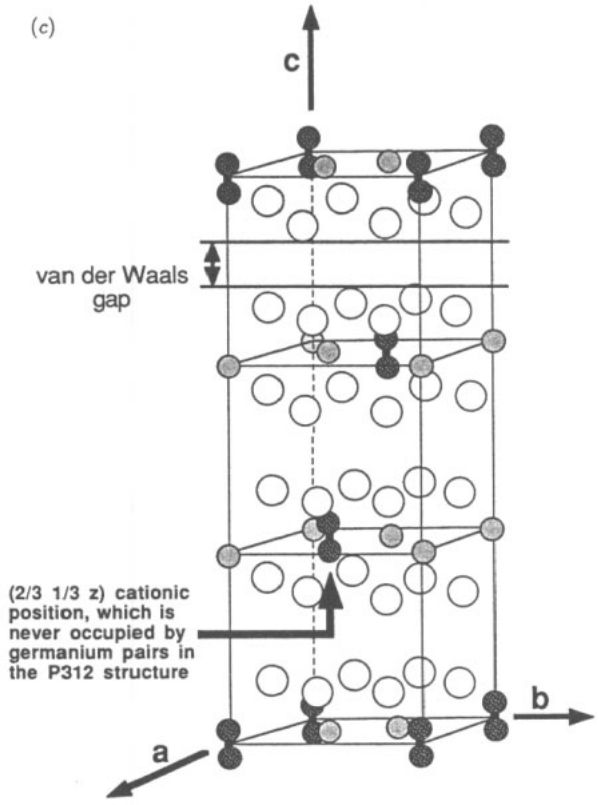

Figure 1. Crystallographic structure of $Cr_2Ge_2Te_6$. (*a*) The cationic distribution within the slab, which is identical for $Cr_2Ge_2Te_6$ single crystals and powder compounds. Note that, owing to the presence of large Ge_2 pairs, $CrTe_6$ octahedra are strongly distorted. (*b*) The stacking sequence observed for $Cr_2Ge_2Te_6$ crystals, leading to the trigonal space group P312. (*c*) The stacking sequence for powdery $Cr_2Ge_2Te_6$, corresponding to the rhombohedral $R\bar{3}$ symmetry.

from crystallographic refinement between the $Cr_2Ge_2Te_6$ powder and single crystals lies in two different cationic distributions from slab to slab. Whereas in the $Cr_2Ge_2Te_6$ powder structure, the chromium atoms and germanium pairs occupy successively each possible cationic position $(\frac{2}{3}\frac{1}{3}z, \frac{1}{3}\frac{2}{3}z, 0\,0\,z)$ from plane to plane, according to the rhombohedral symmetry, the cationic position $(\frac{2}{3}\frac{1}{3}z)$ is never occupied by germanium pairs in the single-crystal structure. This breaks down the rhombohedral symmetry, dropping the structure symmetry to the trigonal symmetry (P312 space group). The occurrence of two different structural symmetries will be discussed in detail in section 3.3. Figure 1(*c*) presents the rhombohedral structure of powdery $Cr_2Ge_2Te_6$.

Table 5 presents the main interatomic distances and bond angles for $Cr_2Ge_2Te_6$. The germanium pair (0.245 92(6) nm) is longer than the silicon pair (0.226 5(7) nm) in isostructural $Cr_2Si_2Te_6$, which can be related to the larger ionic radius for germanium (0.042 nm and 0.053 nm for Si^{4+} and Ge^{4+}, respectively, as Si^{3+} and Ge^{3+} ionic radii are not tabulated). Note also that, owing to the presence of this long germanium pair, Te–Te distances are longer in Ge_2Te_6 octahedra (mean $d_{Te-Te} = 0.382(1)$ nm) than in $CrTe_6$ octahedra (mean $d_{Te-Te} = 0.373(1)$ nm). As always observed for $M_2X_2Te_6$ compounds

Table 3. Data collection and structure calculation for powdery $Cr_2Ge_2Te_6$.

Physical and crystallographic data	
Chemical formula	$Cr_2Ge_2Te_6$
Molecular mass	1014.81 g mol^{-1}
Colour	Medium grey
Crystal symmetry	Rhombohedral
Space group	$R\bar{3}$
Cell parameters at 293 K (refined using x-ray INEL diffractometer powder data)	
a	0.682 75(4) nm
b	0.682 75(4) nm
c	2.056 19(9) nm
V	0.8301(1) nm^3
Z	3
Calculated density d_{calc}	6.091 g cm^{-3}
Data collection	
Temperature	293 K
Radiation	Neutron beam, $\lambda = 0.2425$ nm
Flux	1.5×10^6 neutrons cm^{-2} s^{-1}
Spectrometer	G4.1 (LLB)
Monochromator	Graphite 002
PSD	$17° < 2\theta < 97°$
Refinement conditions	
N − P + C	447
Number of refined parameters	14
Reliability factors	
Fullprof factors	
R_{exp}	0.0505
Bragg R factor	0.0621
Conventional factors	
R_p	0.177
R_{wp}	0.179
R_c	0.0505

Table 4. $Cr_2Ge_2Te_6$ neutron powder pattern atomic coordinates and their estimated standard deviations (space group, $R\bar{3}$).

Atom	Wyckoff position	x	y	z	B_{eq} (Å^2)
Te	18(f)	0.663(1)	−0.033(1)	0.2482(5)	0.5
Cr	6(c)	0	0	0.3302(1)	0.5
Ge	6(c)	0	0	0.0590(6)	0.5

(see, e.g., [16]), one of the two tellurium triangles (one point up and the other down) belonging to two successive anionic planes and which form the $CrTe_6$ octahedron is rotated from its ideal position by an angle of 14°. This is because $CrTe_6$ octahedra have an anisotropic environment, constituted by three 'small' $CrTe_6$ octahedra and three 'large' Ge_2Te_6 octahedra, and this rotation makes the compound able to accommodate octahedra of two different sizes. Furthermore, the mean Te–Te distance (0.377(1) nm) indicates also that $Cr_2Ge_2Te_6$ presents no anionic polymerization, as sometimes observed in tellurides [22].

Table 5. Main distances and angles for $Cr_2Ge_2Te_6$.

Atoms	Distance (nm)
Te–Te	0.374 2(5)
Te–Te	0.373 4(6)
Te–Te	0.383 4(5)
Mean Te–Te	0.377
Cr–Te	0.275 7(7)
Cr–Te	0.274 1(7)
Mean Cr–Te	0.274 9
Cr–Cr	0.394 20(5)
Ge–Te	0.387 6(7)
Ge–Te	0.257 8(4)
Ge–Ge	0.245 92(6)
	Angles (deg)
Te–Cr–Te	85.2(3)
Te–Cr–Te	88.4(3)
Te–Cr–Te	101.1(5)
Te–Cr–Te	86.1(4)
Cr–Te–Cr	44.3(4)
Cr–Te–Cr	33.5(3)
Cr–Te–Cr	20.7(4)
Cr–Te–Cr	91.6(3)
Ge–Ge–Te	38.58(1)
Ge–Ge–Te	100.6(7)
Te–Ge–Te	68.9(2)
Te–Ge–Te	141.4(1)
Te–Ge–Te	79.5(5)
Te–Ge–Te	116.7(6)

3.3. Growth defects evidence and high-resolution electron microscopy investigations

As mentioned before, the different structural symmetries observed for $Cr_2Ge_2Te_6$ powder and single crystals are due to the occupancy, or lack of occupancy, of the cationic ($\frac{2}{3}\frac{1}{3}z$) position by germanium pairs. This indicates that one (or more) phenomenon occurs during crystal growth that breaks the rhombohedral symmetry observed for the powder. The only conceivable phenomenon lies in growth defects. In fact, as the lower trigonal symmetry is not observed for the 50 μm screened grounded $Cr_2Ge_2Te_6$ powder, it seems obvious that these growth defects occur when the single crystals reach sizes larger than at least 50 μm. In order to investigate whether defects are effectively observable or not in $Cr_2Ge_2Te_6$ crystals, we used HREM images, obtained with a CM30 Philips microscope (300 kV). As $Cr_2Ge_2Te_6$ crystals are platelet shaped, they lie flat on the microscope sample holder and we encountered difficulties in investigating other crystallographic planes than the basal plane ((a, b) plane). Comparing high-resolution images of the basal plane (figure 2) with the simulation for the perfect plane calculated with the EMS program [23] and considering our structural results,

we observed very good agreement, giving evidence for a perfect atomic arrangement in the hexagonal (a, b) planes. These calculations, based on multislice wavefunctions, have been made with a defocus of $D_f = 100$ mm, a spherical aberration coefficient $C_s = 2$ mm, and a sample thickness of 6.2 nm (which is rather low, but in agreement with the two-dimensionality of $Cr_2Ge_2Te_6$). In fact, this 6.2 nm thickness corresponds exactly to a sample three cells thick. Such a thickness is too small for investigating stacking faults but is convenient for our investigation of in-plane defects. The good agreement between high-resolution images and simulation calculations for the (a, b) plane (even for higher-scale images), always encountered for all microcrystals systematically studied, indicates the absence of in-plane defects. Then, defects should be stacking defects. Moreover, stacking defects have been observed in compounds presenting structures very close to those of $Cr_2Ge_2Te_6$ [18]. As they drop the structure symmetry from the rhombohedral $R\bar{3}$ space group to the trigonal P312 space group, these systematic stacking defects should be described in terms of $(\frac{2}{3}\frac{1}{3}0)$ translations or $(\pm\pi/3)$ rotations of some successive cationic planes from their 'ideal' position (where the position referred to as 'ideal' corresponds to cations standing on the positions expected in the rhombohedral symmetry). One of the simplest ways to describe these growth defects consists in $(a/-a)$ twinning along the a axis of the cell.

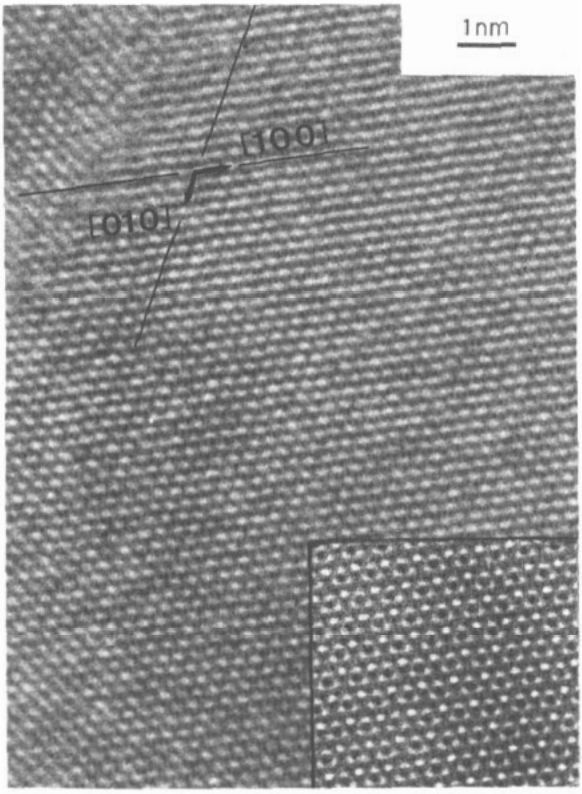

Figure 2. HREM image and simulation for $Cr_2Ge_2Te_6$ basal plane (a, b). [100] and [010] directions are indicated, the lengths of the arrows corresponding to the cell parameter $a = b = 0.6827$ nm. The image simulation, provided in the inset, was calculated using a sample thickness of 6.2 nm, a defocus $D_f = -100$ nm and a spherical aberration coefficient $C_s = 2$ mm.

4. Magnetic properties

The magnetic susceptibility was first measured using the Faraday method, for temperatures from 4.2 to 300 K. Figure 3 presents the thermal evolution of direct and inverse magnetic susceptibilities for $Cr_2Ge_2Te_6$ and indicates a ferromagnetic behaviour with a transition temperature of around 65 K. The experimental value calculated for the effective moment in the paramagnetic domain of the curve, $\mu_{eff} = 3.77\mu_B$, is in good agreement with the theoretical value expected for a Cr^{3+} ion ($3.87\mu_B$). The hysteresis cycle of $Cr_2Ge_2Te_6$ (magnetization versus applied magnetic field) presents a very low remanent magnetization $\sigma_r = 0.1015(5)\mu_B$ and a coercive force $H_c = 34(2) \times 10^{-4}$ T. The magnetization versus temperature curve (figure 4) reveals an interesting behaviour; one can observe a significant magnetization above the 3D ordering temperature. As no magnetic impurity has been detected, this phenomenon could be related to short-range 2D magnetic ordering. At low temperatures, the magnetization saturates and reaches the following value: $\sigma_{5\,K} = 2.92(5)\mu_B$, which is in very good agreement with the expected value for chromium atoms presenting three unpaired electrons ($3\mu_B$). In order to determine accurately the Curie temperature, the method of Belov and Goryaga [24] and Kouvel [25] has been used. According to this method, the transition temperature is determined unequivocally by the isothermal H/σ versus σ^2 curve passing through the origin and is equal to 61(1) K. The neutron diffraction study (figure 5) shows that the magnetic peaks (corresponding to magnetic ordering) disappear at 61(1) K, which is in excellent agreement with the transition temperature deduced from Belov and Goryaga–Kouvel curves. However, no residual magnetization is observed above T_C for the neutron study (see figure 7 later), whereas some was observed in the magnetometer study (figure 4). This contradiction between these two magnetization versus temperature curves is puzzling, but we have to date no tentative explanation to propose.

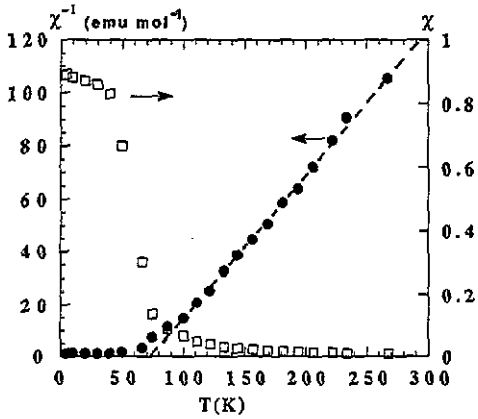

Figure 3. Thermal evolution of direct and inverse magnetic susceptibility of $Cr_2Ge_2Te_6$. The curves have been corrected for core magnetism.

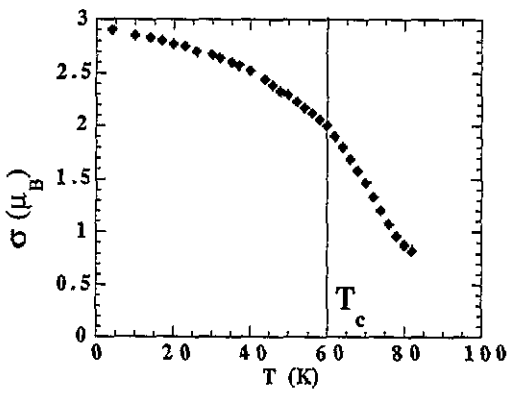

Figure 4. Thermal evolution of the magnetization. The presence of a significant magnetization above T_C could be related to 2D short-range magnetic order.

5. Magnetic structure

The diffraction patterns were analysed by the Rietveld–Hewat [19, 20] method as modified

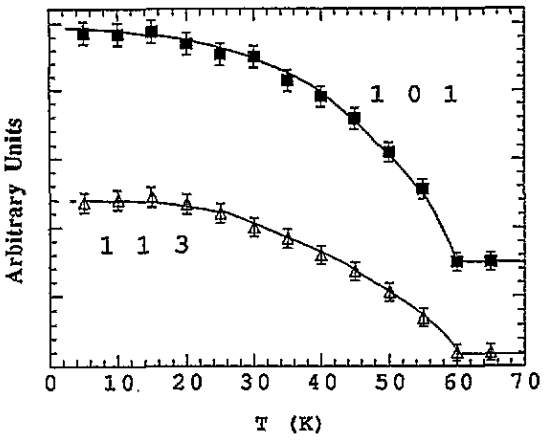

Figure 5. Thermal evolution of the integrated intensities of two magnetic peaks. The intensities variation indicates a Curie temperature of 61(1) K.

by Wiles *et al* [26]. The nuclear scattering lengths and magnetic form factors were taken from the work of Sears [27] and Watson and Freeman [28], respectively. Bertaut's [29] representation theory was used to identify the possible magnetic structure models. Neutron diffraction diagrams were collected at various temperatures between 5 and 70 K, and the thermal evolution of some magnetic peaks appears in figure 5. This indicates that the Curie temperature corresponds to the minimum of $\chi^{-1}(T)$ observed at 61 K. Below 61 K, magnetic contributions appear which superimpose on the pre-existing Bragg peaks due to the nuclear cell. Furthermore, the absence of any magnetic contribution on the (001) reflections gives strong evidence for moments lying along the c axis of the cell.

The magnetic structure has been solved using Bertaut's [29] representation analysis. For the $R\bar{3}(k=0)$ space group, the irreducible representations given in table 6 lead to the modes listed in table 7.

Table 6. Irreducible representations of $R\bar{3}(k=0)$. $w=\exp(2\pi i/3)$.

	E	C_3	C_3^2	I	S_6	S_6^5
Γ_1	1	1	1	1	1	1
Γ_2	1	1	1	−1	−1	1−
Γ_3	1	w	w^*	1	w^*	w
Γ_4	1	w^*	w	1	w	w^*
Γ_5	1	w	w^*	−1	$-w^*$	$-w$
Γ_6	1	w^*	w	−1	$-w$	$-w^*$

Table 7. Bertaut's mode for $Cr_2Ge_2Te_6$. The 6c cation position is taken from the *International Table of Crystallography* (space group, No.148).

	$x\,0\,y$ plane	z
Γ_1	—	$S_{1z}+S_{2z}+S_{3z}-S_{4z}-S_{5z}-S_{6z}$
Γ_2	—	$S_{1z}+S_{2z}+S_{3z}+S_{4z}+S_{5z}+S_{6z}$
Γ_3	—	—
Γ_4	$S_{1x}+S_{2x}+S_{3x}-S_{4x}-S_{5x}-S_{6x}$	—
Γ_5	—	—
Γ_6	$S_{1x}+S_{2x}+S_{3x}+S_{4x}+S_{5x}+S_{6x}$	—

Γ_4 and Γ_6 representations are ruled out because they lead to a star configuration of spins within the (a, b) plane. Only the Γ_1 and Γ_2 representations are convenient for moments lying along the c axis of the cell. As the Γ_1 representation corresponds to antiferromagnetic behaviour, it can also be ruled out. The Γ_2 representation corresponds to ferromagnetic behaviour, due to the collinear configuration of spins lying along the c axis of the cell.

Atomic positions and spin components were refined simultaneously for each temperature. As expected, the best fit ($R_{mag} = 0.0797$ at 5 K) corresponds to the Γ_2 mode. Spin components and atomic coordinates are listed in table 8. The comparison between the calculated and observed patterns is given in figure 6. Cr^{3+} spins (figure 7) exhibit a value ($\mu = 2.80(4)\mu_B$ at 5 K) which is in good agreement with the magnetic study. Figure 8 shows the thermal evolution of cell parameters of $Cr_2Ge_2Te_6$, indicating the occurrence of a strong magnetostriction at the ferromagnetic ordering.

Table 8. Atomic coordinates of $Cr_2Ge_2Te_6$ at 270 K (paramagnetic state) and at 5 K (ferromagnetic state). At 270 K, $a = 0.6809(1)$ nm and $c = 2.0444(3)$ nm; at 5 K, $a = 0.68196(7)$ nm and $c = 2.0371(3)$ nm. The refined cell parameters are $R_{nucl} = 0.0778$ for 270 K and $R_{nucl} = 0.0503$ and $R_{mag} = 0.0787$ for 5 K.

Temperature (K)	State	Atom	Position	x	y	z	B_{eq} ($\times 10^2$ nm^2)
270	Paramagnetic	Cr	6(c)	0	0	0.3302(6)	0.30
5	Ferromagnetic	Cr	6(c)	0	0	0.3339(5)	0.15
270	Paramagnetic	Ge	6(c)	0	0	0.0590(5)	0.30
5	Ferromagnetic	Ge	6(c)	0	0	0.0601(5)	0.15
270	Paramagnetic	Te	18(f)	0.663(1)	−0.033(1)	0.2482(5)	0.30
5	Ferromagnetic	Te	18(f)	0.665(1)	−0.036(1)	0.2499(6)	0.15

6. Electronic properties and band structure

$Cr_2Ge_2Te_6$ room-temperature resistivity has been measured on single-crystal platelets up to centimetre size. At room temperature, $Cr_2Ge_2Te_6$ exhibits a $\rho = 0.02\ \Omega$ cm resistivity. Thermal evolution of the resistivity of $Cr_2Ge_2Te_6$ has been studied using the Montgomery [13] method and is reported in figure 9. At high temperatures ($T > T_C$), the resistivity behaviour can be fitted as $\rho = \exp(A/kT)$, where k is the Boltzmann constant and $A = 0.2$ eV. As expected, an irregularity in the curve is clearly visible at the transition temperature, resulting in a drastic change in the curve slope (from $A = 0.2$ eV to about 7 meV). The fact that this transition does not occur suddenly but is progressive can be related to the two-dimensionality of the $Cr_2Ge_2Te_6$ structure. The high-temperature electronic behaviour of $Cr_2Ge_2Te_6$ (ρ varying exponentially with $1/T$) could correspond to either a semiconducting or a Mott insulator-like behaviour. If we consider the usual definition of a semiconductor, $Cr_2Ge_2Te_6$ should not be considered as a semiconducting material, as it presents some unpaired electrons. We can then conclude that $Cr_2Ge_2Te_6$, which is ferromagnetic at low temperatures ($T < T_C$), exhibits for high temperatures ($T > T_C$) a resistivity controlled by a hopping conduction phenomenon (where A can be considered as an activation energy). For temperatures below T_C, the resistivity is also governed by an exponential law, but the so-called 'activation energy' A is far smaller than in the paramagnetic state (7 meV compared with 0.2 eV). A tentative explanation could be given in terms of electron conduction 'channels', as often observed in magnetic multi-layer magnetic

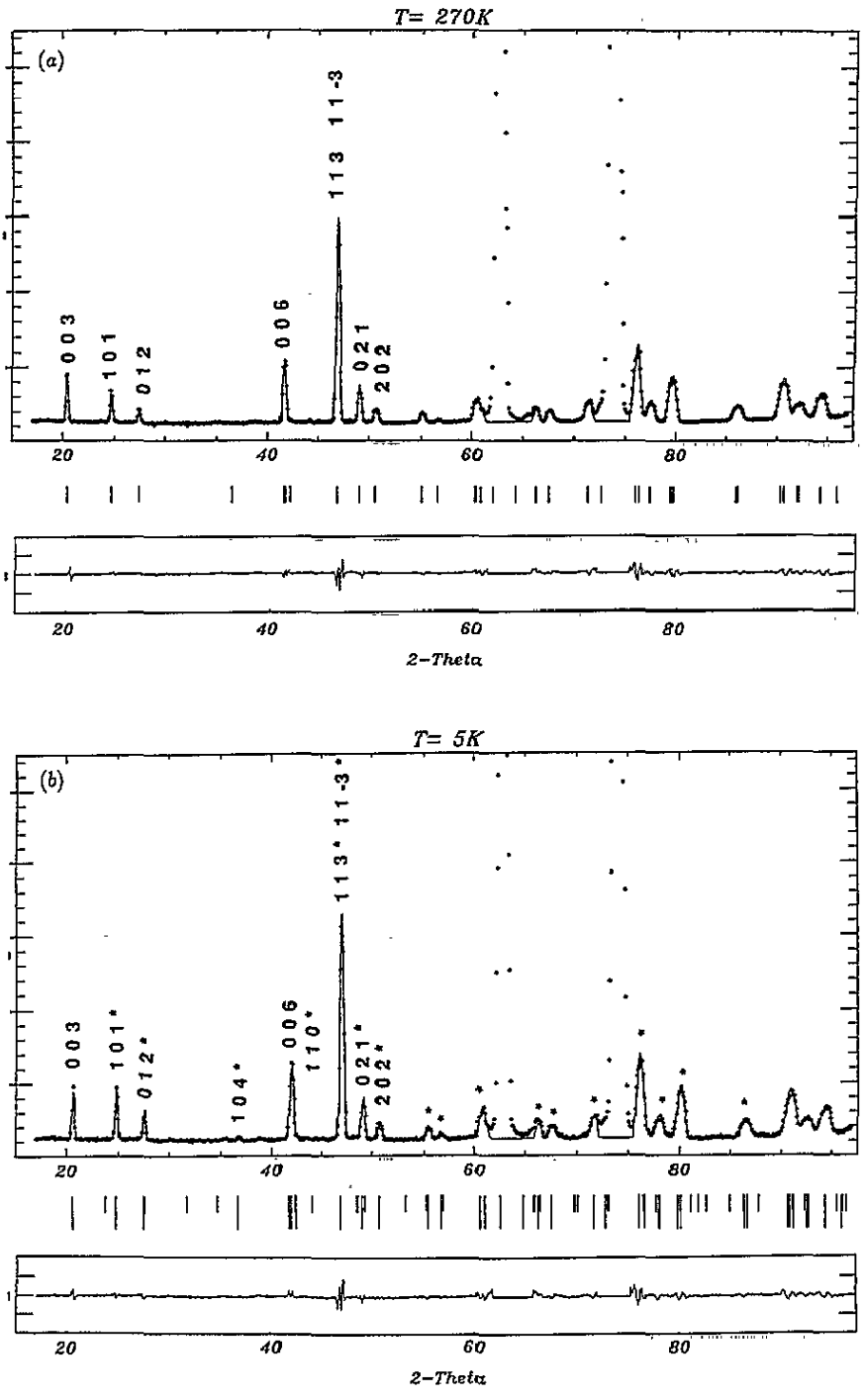

Figure 6. Comparison between observed and calculated intensities of diffraction patterns in (*a*) the paramagnetic state (270 K) and (*b*) ferromagnetic state (5 K): * magnetic contributions. For clarity, *hkl* have been omitted for $2\Theta > 55°$. 2Θ regions containing aluminium peaks (due to the sample holder and to the cryostat) are excluded for calculations.

systems [30]. Let us consider two conduction channels for the conduction electrons: the first for the 'up' electrons, and the second for the 'down' electrons. A possible explanation would be that, in the paramagnetic state, these two channels are characterized by the same resistance, whereas they exhibit different resistances in the ferromagnetic state. One channel (e.g. the 'down'-electron channel) could interact with the ordered spins and present a far higher resistance than the other ('up'-electron channel), which could be unaffected by the magnetic ordering. In the global resistivity behaviour, mostly the smaller resistance effect would occur in the activation energy for the ferromagnetic state.

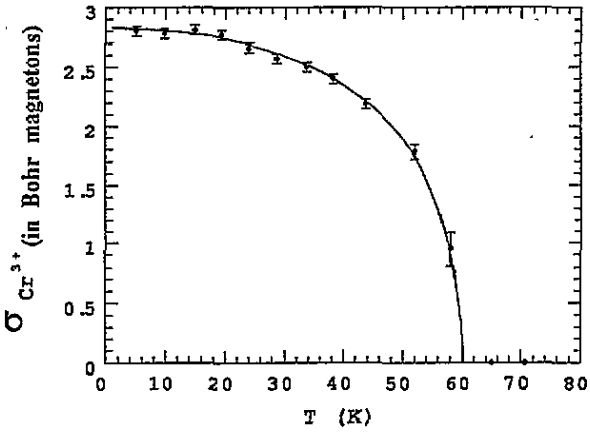

Figure 7. Thermal evolution of the refined magnetic moments of Cr^{3+}.

In order to confirm the hopping mechanism assumed for $Cr_2Ge_2Te_6$ electronic conduction, we calculated the band structure of $Cr_2Ge_2Te_6$, using the extended Hückel method [31] (an LCAO method). We considered the equivalent rhombohedral cell ($a = b = c = 0.7907$ nm and $\alpha = \beta = \gamma = 51.16°$) to restrict the number of variables and the length and complexicity of calculations. Figure 10 presents the global density of states of $Cr_2Ge_2Te_6$ and the contribution of each atom type. The Fermi level E_F equals 11.86 eV and corresponds to a very sharp peak in the density of states. Close examination of contributions from the different atoms of the cell indicates that this peak is mostly due to chromium 3d orbitals (t_{2g}). The sharpness of the peak and the high density of states at the Fermi level give strong evidence for a localized electronic system. We can also notice the presence of a non-negligible tellurium 5p contribution, in the same energy range as the high Cr 3d contribution. These tellurium 5p orbitals could then play a role in magnetic Cr–Cr couplings. Figure 11 presents the crystal orbital dispersion in the $\Gamma\Lambda'$ direction of the rhombohedral first Brillouin zone. Note that the band width is very small at the Fermi level (about 1 eV), indicating a strongly localized electronic system, consistent with the hypothesis of 'Mott insulator-like' behaviour for $Cr_2Ge_2Te_6$. At $k = 0$ (Γ point) and at the Fermi level, three crystal orbitals exist, which are very close to each other (they are separated by only 0.3 eV). There is a 'chromium 3d orbital' (due mostly to chromium t_{2g} states), surrounded by two '5p orbitals' due to the tellurium atoms. This situation, with a ligand orbital lying just above a metal orbital at the Fermi level, is rather unusual. Because of the weak correlation energy U_p of tellurium, this upper ligand orbital could be occupied. One electron from this level could also be excited to the e_g chromium free states, which could be related to the possibility of Cr–Te–Cr superexchange between chromium atoms through tellurium orbitals.

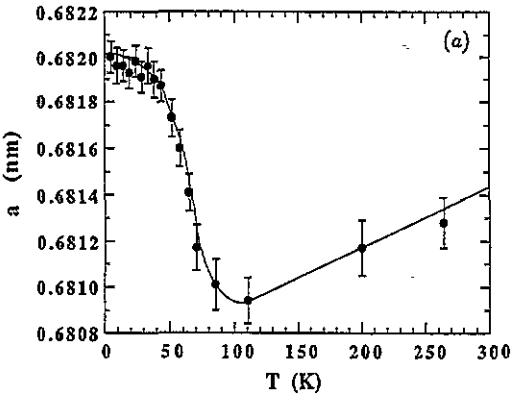

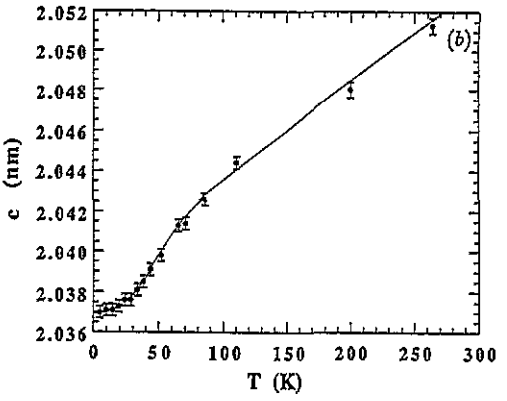

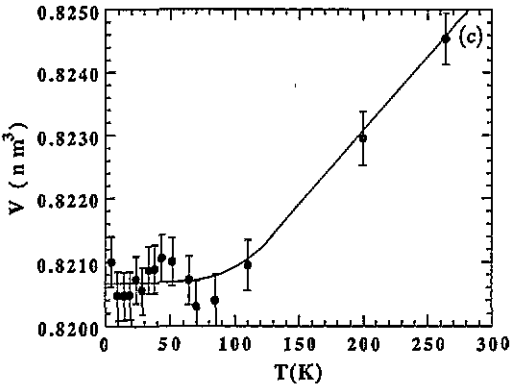

Figure 8. Thermal evolution of $Cr_2Ge_2Te_6$ cell parameters: (*a*) evolution of *a*; (*b*) evolution of *c*; (*c*) evolution of the volume of the hexagonal cell.

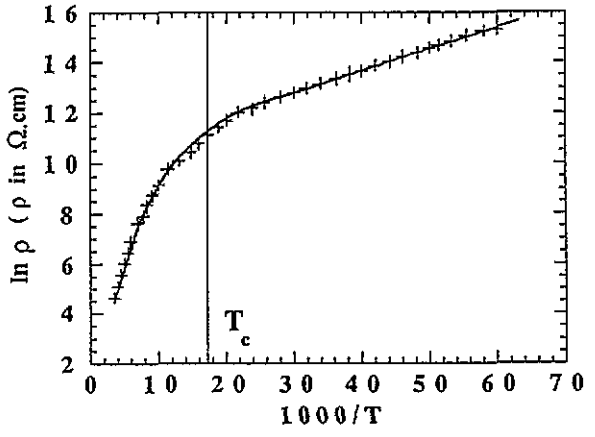

Figure 9. Thermal evolution of $Cr_2Ge_2Te_6$ resistivity.

7. Discussion

One of the most interesting characteristics of $Cr_2Ge_2Te_6$ compared with its isostructural silicon parent compound $Cr_2Si_2Te_6$ is its very different ferromagnetic temperature, 61(1) K for the germanium compound compared with 32(1) K for the silicon derivative. The first and simplest explanation of this difference lies in steric effects; in fact, Ge_2 pairs

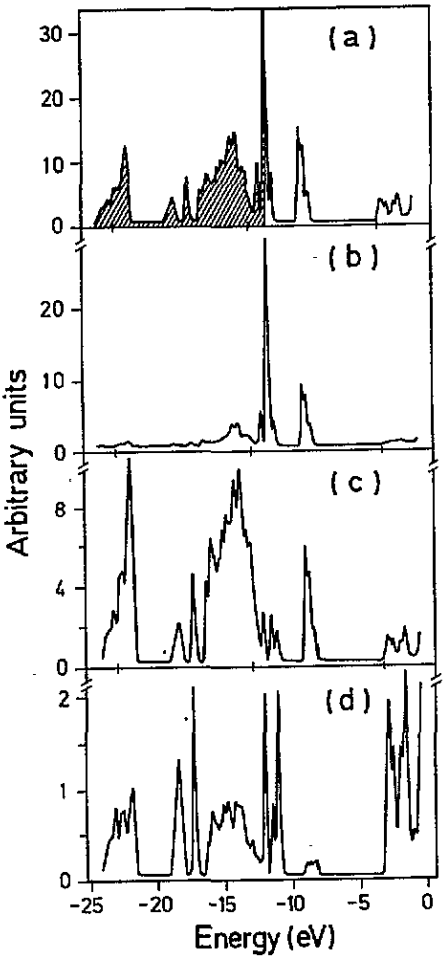

Figure 10. (*a*) Global density of states for $Cr_2Ge_2Te_6$ and (*b*)–(*d*) contributions from the different atom types: (*b*) chromium atom contribution; (*c*) tellurium atom contribution; (*d*) germanium atom contribution. Arbitrary units are given for comparison the magnitudes of the contribution from each atom type.

in $Cr_2Ge_2Te_6$ are much longer than silicon pairs in $Cr_2Si_2Te_6$ (0.245 92(6) nm and 0.226 5(7) nm respectively). This induces for $Cr_2Ge_2Te_6$ larger (Ge_2Te_6) octahedra than (Si_2Te_6) in $Cr_2Si_2Te_6$ (d_{Ge-Te} = 0.257 8(9) nm and d_{Si-Te} = 0.250 8(7) nm), and consequently smaller ($CrTe_6$) octahedra in $Cr_2Ge_2Te_6$ (mean d_{Cr-Te} = 0.274 4(2) nm in $Cr_2Ge_2Te_6$, and mean d_{Cr-Te} = 0.278(1) nm in $Cr_2Si_2Te_6$). Furthermore, these ($CrTe_6$) octahedra are more distorted in the germanium compound than in the silicon isotype (the distortion angle varies from 8.1° for $Cr_2Si_2Te_6$ to 14.4° for $Cr_2Ge_2Te_6$). Let us consider two chromium atoms linked by a tellurium atom in such an outline that ferromagnetic superexchange is favoured (i.e. with an angle Cr(1)–Te–Cr(2) of around 90°) in the silicon and germanium compounds. In $Cr_2Si_2Te_6$, the three typically encountered distances are $d_{Cr(1)-Te}$ = 0.2751 nm, $d_{Cr(2)-Te}$ = 0.277 nm, and $d_{Cr(1)-Cr(2)}$ = 0.3909 nm, and the Cr(1)–Te–Cr(2) angle is 90.4°. In $Cr_2Ge_2Te_6$, the distances are $d_{Cr(1)-Te}$ = 0.273 nm, $d_{Cr(2)-Te}$ = 0.275 nm and $d_{Cr(1)-Cr(2)}$ = 0.3942 nm and the angle is Cr(1)–Te–Cr(2)=91.6°.

Concurrently, the van der Waals gap is slightly smaller in $Cr_2Ge_2Te_6$ than in $Cr_2Si_2Te_6$ (0.335 nm and 0.344 nm, respectively). These two phenomenon (larger (Ge_2Te_6) octahedra and smaller gap) could explain the enhancement of T_C from the silicon compound to the germanium compound. In fact, on the assumption classically that direct planar chromium–

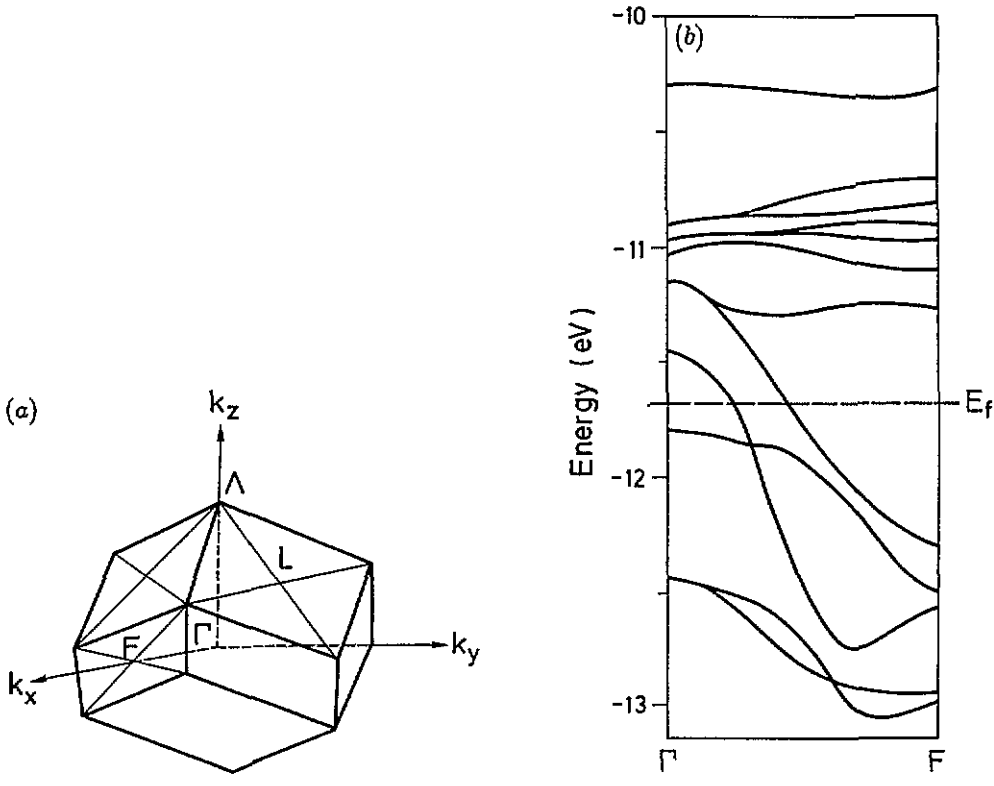

Figure 11. (*b*) Crystal orbital dispersion in the $\Gamma\Lambda'$ direction of the rhombohedral first Brillouin zone. (*a*) A representation of the first Brillouin zone for rhombohedral $Cr_2Ge_2Te_6$.

chromium interactions are antiferromagnetic, and that ferromagnetic exchanges are due to planar and inter-planar superexchange Cr–Te–Cr interactions, the above-mentioned steric effects will reduce direct antiferromagnetic Cr–Cr interactions and favour ferromagnetic superexchange interactions. Larger (Ge_2Te_6) octahedra will increase the planar Cr–Cr distances in $Cr_2Ge_2Te_6$ ($d_{Cr-Cr} = 0.3909(2)$ nm for $Cr_2Si_2Te_6$ and $d_{Cr-Cr} = 0.39347(4)$ nm for $Cr_2Ge_2Te_6$) and so reduce the antiferromagnetic component of the exchange interaction between first neighbours Cr–Cr. Furthermore, the smaller gap in $Cr_2Ge_2Te_6$ will increase inter-planar couplings. These two convergent phenomena could explain the enhancement of the Curie temperature from 32(1) K for the silicon derivative to 61(1) K for the germanium compound.

The precise magnetic study of $Cr_2Si_2Te_6$ and $Cr_2Ge_2Te_6$ using elastic and inelastic neutron scattering is currently in progress at the Laboratoire Léon Brillouin at Saclay. Interesting results have been obtained, indicating a strongly anisotropic 2D Ising-like behaviour for $Cr_2Si_2Te_6$.

Acknowledgments

The authors are very indebted to J L Mansot (IMN, Nantes) for his help with the HREM techniques, to Dr Chen and P Monceau (CRTBT, Grenoble) for displaying the

low-temperature resistivity measurements, and to Dr J C Grenier (CNRS, Bordeaux) for perfoming the magnetization measurements.

References

[1] Brec R 1986 *Solid State Ion.* **22** 3
[2] Ouvrard G, Sandré E and Brec R 1988 *J. Solid State Chem.* **73** 23
Marsh R E 1988 *J. Solid State Chem.* **77** 190
[3] Carteaux V, Ouvrard G, Grenier J C and Laligant Y 1991 *J. Magn. Magn. Mater.* **94** 127
[4] Carteaux V 1992 *Thesis* University of Nantes
[5] Odink D A, Carteaux V, Sandré E and Ouvrard G 1993 *Chem. Mater.* **5** 237
[6] Jobic S, Le Boterf P, Bedenan F and Ouvrard G 1994 *C. R. Acad. Sci. Paris II* **318** 893
[7] Jobic S, Le Boterf P, Brec R and Ouvrard G *J. Alloys Compounds* **205** 139
[8] Deniard P, Evain M, Barbet J M and Brec R 1991 *Mater. Sci. Forum* **79** 363
[9] Yvon R, Jeitschko W and Parthe E 1977 *J. Appl. Crystallogr.* **10** 73
[10] Kay Fair C 1990 *Structure Determination System Enraf–Nonius*
[11] van der Pauw L J 1958 *Phillips Tech. Rev.* **20** 220
[12] van der Pauw L J 1961 *Phillips Res. Rep.* **16** 187
[13] Montgomery H C 1971 *J. Appl. Phys.* **42** 2971
[14] Walker N and Stuart D 1983 *Acta Crystallogr.* A **39** 158
[15] Hamilton W C 1965 *Acta Crystallogr.* **18** 502
[16] Sandré E, Carteaux V and Ouvrard G 1992 *C. R. Acad. Sci., Paris, II* **314** 1151
[17] Sandré E, Carteaux V, Marie A M and Ouvrard G 1994 *J. Alloys and Compounds* **204** 145
[18] Fragnaud P, Prouzet E and Brec R 1992 *J. Mater. Res.* **7** 1839
[19] Rietveld H M 1969 *J. Appl. Crystallogr.* **2** 65
[20] Hewat A W 1973 *Harwell Rep.* AERE R 7350
[21] Rodriguez-Carvajal J 1990 *Abstracts Satellite Meet. on Powder Diffraction of the 15th Congr. of the International Union of Crystallography (Toulouse, 1990)* p 127
[22] Canadell E, Jobic S, Brec R and Rouxel J 1992 *J. Solid State Chem.* **98** 59
[23] Stadelman P 1987 *Ultramicroscopy* **21** 131
[24] Belov K P and Goryaga A N 1956 *Fiz. Metall. Metalloved.* **2** 3
[25] Kouvel J S 1957 *General Electric Research Laboratory Rep.* **59** 1799
[26] Wiles D B, Young R A and Sakthivel A 1981 *J. Appl. Crystallogr.* **14** 149
[27] Sears V F 1992 *Neutron News* **3** 26
[28] Watson R E and Freeman J 1961 *Acta Crystallogr.* **14** 27
[29] Bertaut E F 1968 *Acta Crystallogr.* **24** 217
[30] Fert A 1994 Private communication
[31] Whangbo M H and Evain M 1987 Department of Chemistry, North Carolina University, Raleigh, NC